https://doi.org/10.1016/j.ijmecsci.2019.105200

Analysis of size dependent earing evolution in micro deep drawing of TWIP steel by using crystal plasticity modelling

N. Guo [a], C. Y. Sun [b, *], Y. F. Zhang [c], M. W. Fu [d, #]

[a] School of Mechanical and Automotive Engineering, Qilu University of Technology (Shandong Academy of Sciences), Jinan, 250353, China

[b] School of Mechanical Engineering, University of Science and Technology Beijing, Beijing, 100083, China

[c] Institute of Microstructure and Property of Advanced Materials, Beijing University of Technology, Beijing, 100124, China

[d] Department of Mechanical Engineering, The Hong Kong Polytechnic University, Hung Hom, Kowloon, Hong Kong

Abstract

As a promising microforming process, micro deep drawing has attracted great attention for manufacturing of microparts with unique cup-features. However, the occurrence of size effect (SE) and the intrinsic characteristics of crystallographic orientation can lead to an inevitable and uncertain plastic anisotropy during the micro deep drawing and further result in the formation of earing. In this research, a size dependent crystal plasticity (CP) model considering the interactions between slip and twinning was developed via incorporating the size scaling factor into the surface layer model to represent and model the SE and further analyze the entire micro deep drawing process of the TWIP steel. Then the micro deep drawing of polycrystalline TWIP steel with different grain sizes and thicknesses was conducted using the elaborately designed tooling sets. The size dependent crystal plasticity-based finite element modelling in conjunction with a virtual polycrystalline microstructure was employed to study the earing evolution induced by grain size, orientation and

geometrical size. It is revealed that an obvious earing profile occurred in the workpiece with the larger size scaling factor. In addition, it is noted that the earing at micro scale is obviously higher than that at macro scale. The asymmetric distribution of earing profile is induced by the Goss and Brass orientations, while the Cubic type orientation leads to the symmetric distribution of earing profile. This issue is mainly attributed to the symmetric distribution of slip activities than that of twinning activities, since the activated quantity of twinning volume fraction is much smaller. Therefore, the proposed size dependent crystal plasticity modelling is efficient in predicting the earing formation at micro scale. The study thus provides an in-depth understanding of micro deep drawing of sheet metals and accurate prediction of shape microforming of microparts.

Keywords: Size effect; Earing; Crystal plasticity; TWIP steel; Micro deep drawing

Corresponding authors:

*C.Y. Sun: Tel.: +86-010-62333695, E-mail: suncy@ustb.edu.cn

#M.W. Fu: Tel: +852-27665527, E-mail: mmmwfu@polyu.edu.hk

1. Introduction

As a sub-set of microforming process, micro deep drawing is referred to fabrication of sheet metal parts via micro-scaled plastic deformation of sheet metal. The process has a promising potential in mass production of micro parts. However, many researches have shown that with the dimensions of parts scaled down to micro scale, the occurrence of size effect (SE) significantly affects the behavior and performance of micro deep drawing process. Vollertsen et al. [1] found that the size effects occurring in microforming process affect the tribological aspects. Cao et al. [2, 3] revealed that the friction condition was nonuniform and showed a dependence on the geometric size of micropin. Fu et al. [4-6] reported that size effects lead to the irregular geometry and rough surface finish of the formed parts. The traditional knowledge established in macro scale forming may not be fully valid and cannot be directly leveraged into the microforming process. In addition, engineering polycrystalline sheet metals often exhibit remarkable elastic-plastic anisotropy at single crystal level that can be attributed to the presence of crystallographic orientations, which is generally believed to be an inevitable side-effect of the materials processed at small scale. Therefore, in-depth understanding of the effects of geometric size and grain orientation on deformation characteristics is crucial in design and development of micro-drawn parts.

Plastic anisotropy, significantly affects the quality of the microformed parts [7], which may entail the formation of uneven rims of the drawn parts, usually referred to as earing during deep drawing that must be trimmed at final stage and leading to higher manufacturing cost. Tang et al. [8] highlighted that the occurrence of the pronounced earing during the final deep drawn process is undesirable as it requires an additional processing step to trim the uneven rim of the drawn cup. Another important consequence is an inhomogeneous distribution of the mechanical properties. In addition, these unknown or negligible effects in macro forming

need to be carefully addressed by experimentation, modelling and simulation at microscopic scale. In microforming, many researches are generally focused on the variational flow stress of materials and other size affected phenomena. Saotome et al. [9] evaluated the drawability in deep drawing of sheet steels with the thickness of 0.05, 0.1, 0.2 and 1.0 mm, and demonstrated that drawability was acquired without a large amount of blank holder pressure for thin sheet steels. Chan et al. [10] revealed that with the decrease of the ratio of specimen to grain sizes, the flow stress is decreased linearly. However, the effects caused by the changes of grain size and geometric dimension on the earing formation and its characteristics have not yet been explored systematically well.

To overcome the limitations of the classical continuum plasticity models in describing the micro scaled deformation behaviors, a series of material models were proposed to address these new challenges numerically based on experimental measurement via incorporating the dependence on specimen dimensions. Xu et al. [11] proposed a constitutive model considering the geometry and grain size effects on the formability of metallic materials during the meso-/micro-scaled forming processes. Molotnikov et al. [12] established a model to illustrate that the strength of interior grains is determined by dislocation cell structure, while that of surface grains is governed by dislocation image forces. Peng et al. [13] developed a phenomenological model considering the ratio of grain size and geometrical size based on the surface layer model. Among these size dependent models, the surface layer model and its modified versions are considered to be a widely used and efficient approach to describing the variation of the overall flow stress in microforming process, as illustrated in the research of Geißdörfer et al. [14]. The key idea of this model is that the specimen is divided into a surface layer and an inner part. The flow stress consists of the contributions from both parts based on their own volume fractions and flow stresses. Although the surface layer model is simple, versatile and robust, Tôth et al. [15] indicated that it has a limited

predictive capability to predict the underlying deformation mechanisms since there are no crystallographic evolutions and grain orientations involved, which play a crucial role in plastic deformation process. Therefore, a microstructural based material model incorporating the SE needs to be established to account for deformation mechanisms and the influence of SE simultaneously in microforming processes.

In addition, Tjahjanto et al. [16] illustrated that since the material anisotropy in micro sheet forming process is strongly related to grain orientation and distribution, the crystal plasticity (CP) model considering the crystallographic orientation distribution of grains could be employed as a multiscale framework to simulate the earing profiles. Walde and Riedel [17] developed a crystal plasticity finite element method (CPFEM) coupling with the texture component to investigate the influence of the major texture components on the earing behavior of a deep-drawn cup. It is demonstrated that the earing pattern depends on the initial texture at the beginning of the drawing process significantly. Furthermore, Tikhovskiy et al. [18] proposed a texture component based CPFEM incorporating the original texture of the material to simulate the deep drawing process of aluminum sheet and to predict the earing behavior in cup drawing considering twelve slip systems and the applicability of the model was further validated. Sun et al. [19] established a CP model considering slip, twinning and transformation to predict the macroscopic strain hardening of TWIP steel. However, the abovementioned CP model has limitation in representing the SE at micro scale since it does not consider SE in the model.

Attempts have therefore been made to incorporate the SE into a phenomenological CP model by Kocks and Mecking [20]. However, Verma and Biswas [21] pointed out that a more practical approach to including the SE in mathematical formulation is to assume that the yield stress depends upon strain gradient. Consequently, strain gradient plasticity theory is employed to describe the SE via calculating the geometrically necessary dislocation, namely

the so-called nonlocal CP model which was established by Acharya and Beaudoin [22]. Furthermore, Zhang and Dong [23] established a nonlocal physically based CP model including statistically stored dislocations, geometrically necessary dislocations on the slip systems to investigate the SE of micro deep drawing process. It is demonstrated that this model provided more microstructural clues for the interpretation of SE in the microforming processes. However, Cheong et al. [24] pointed out these models are incapable of addressing the influence of microstructure and also sensitive to finite element mesh. Meanwhile, the simulations done by employing this model required plenty of time due to the complicated numerical compiling and implementation.

In this research, a twinning-induced plasticity steel (TWIP), viz., TWIP steel was chosen as a case study material. A size dependent CP model considering the interactions between slip and twinning was proposed via incorporating the size scaling factor into the surface layer model to represent the SE. The validation of this proposed CP model was done via comparing the mechanical responses obtained by micro tensile test and simulation. The microstructural morphology and the grain size of TWIP steel were studied via EBSD measurement. The micro deep drawing experiments were conducted using the tailor-designed tooling sets. To study the earing evolution induced by size and grain orientation effects, the set-up of FE model for micro deep drawing was subsequently carried out based on the size dependent CP model. Finally, the influences of grain and geometry size on earing formation and its characteristics at micro scale were analyzed, and the effect of initial grain orientation on earing profiles was identified according to the slip and twinning activities by comparing with that at macroscopic scale. The study therefore provides a theoretical and experimental understanding of earing formation and evolution in micro deep drawing process, which is useful for the integrated design of micro forming process and defect-free micro cups with favorable appearance of TWIP steels.

2. Constitutive description of size dependent CP model

2.1 Formulation of slip and twinning

The framework of CP model considering slip and twinning is described as follows. In the proposed CP model, based on the study of Kalidindi et al. [25], the decomposition of deformation gradient tensor $\mathbf{F}$, is formulated as:

$$\mathbf{F} = \mathbf{F}^e \cdot \mathbf{F}^p \tag{1}$$

where $\mathbf{F}^e$ denotes elastic deformation, while $\mathbf{F}^p$ represents an irreversible permanent plastic deformation. In Fig. 1, the deformation gradient decomposed into the elastic and plastic parts is illustrated associated with the slip and twinning mechanisms.

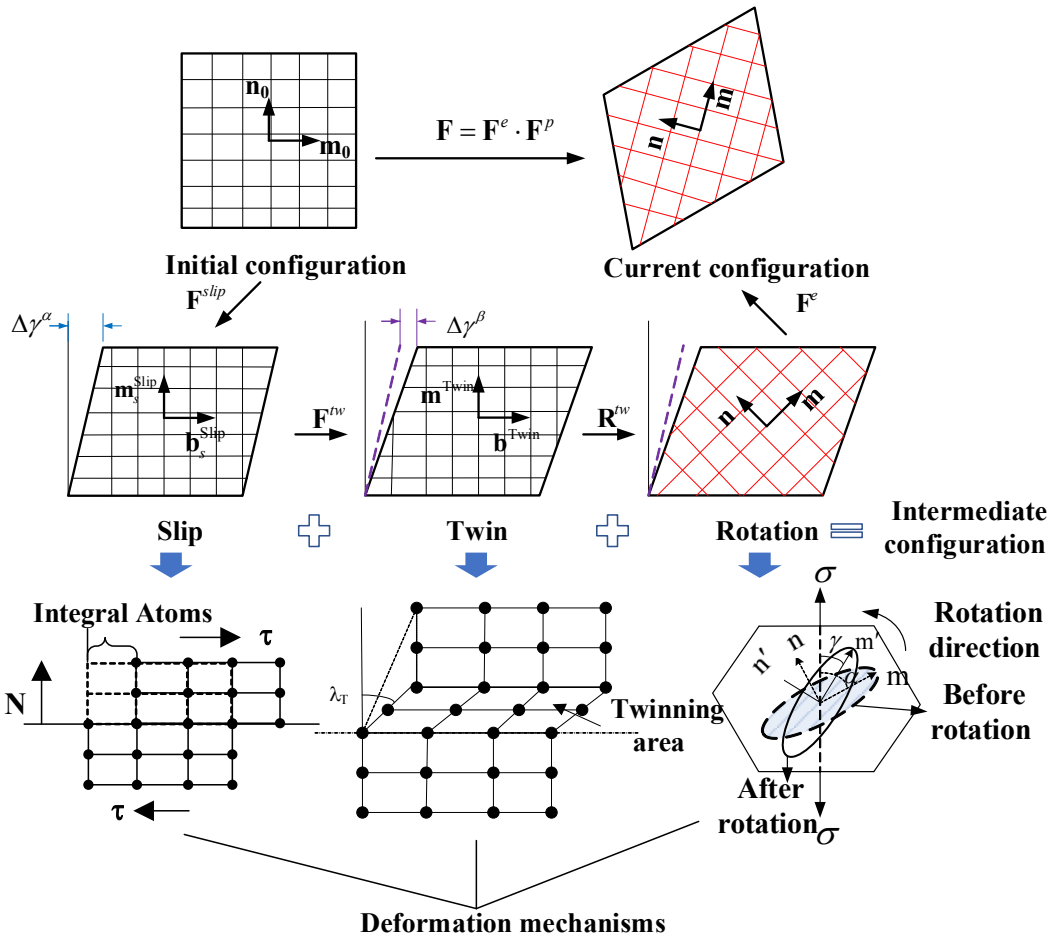

Fig. 1. The decomposition of deformation gradient into the elastic and plastic parts including slip and twin associated with the corresponding deformation mechanisms.

In order to clarify the evolution of finite deformation kinematics, the plastic deformation gradient $\mathbf{F}^p$, illustrated by the plastic velocity gradient $\mathbf{L}_p$ which considering slip and twinning mechanisms, is described by the following:

$$\mathbf{L}_p = \dot{\mathbf{F}}^p \cdot \mathbf{F}^{p^{-1}} = \sum_{\alpha=1}^{N_{slip}} \dot{\gamma}^{\alpha} \mathbf{S}_s^{Slip} + \sum_{\beta=1}^{N_{twin}} \dot{\gamma}^{\beta} \mathbf{S}_t^{Twin} \tag{2}$$

where N_{slip} and N_{twin} are the number of slip systems and twin systems, respectively. $\dot{\gamma}^{\alpha}$ ($\alpha = 1$ to N_{slip}) denotes the shear rate of each possible slip system, $\dot{\gamma}^{\beta}$ ($\beta = 1$ to N_{twin}) represents the twinning shear rate. In addition, $\mathbf{S}_s^{Slip}$ and $\mathbf{S}_t^{Twin}$ describe the Schmid tensor generated by a unit slip on system *s* and a unit twin on system *t*, respectively.

The stress based constitutive equation to represent the elastic stretch is given by:

$$\mathbf{T}^e = \mathfrak{R} : \mathbf{E}^e \tag{3}$$

where $\mathbf{T}^e$ and $\mathbf{E}^e$ represent the symmetric second Piola-Kirchoff (PK) stress and the Green elastic strain, respectively. $\mathfrak{R}$ denotes a fourth-order elasticity tensor. These variables are defined in the following equation:

$$\mathbf{E}^e = \frac{1}{2}(\mathbf{F}^{e^{\mathrm{T}}} \cdot \mathbf{F}^e - \mathbf{I}) \tag{4}$$

The stress measure $\mathbf{T}^e$ is designated as:

$$\mathbf{T}^e = \mathbf{F}^{e^{-1}} \cdot \left\{ \det(\mathbf{F}^e) \cdot \boldsymbol{\sigma} \right\} \cdot \mathbf{F}^{e^{-\mathrm{T}}} \tag{5}$$

where $\boldsymbol{\sigma}$ indicates the Cauchy stress. The resolved shear stress (RSS) τ^{α} associated with the α th slip system is expressed as:

$$\tau^{\alpha} = \boldsymbol{\sigma} : \mathbf{S}^{\alpha} \tag{6}$$

To illustrate the hardening relationship of TWIP steel, the evolution of slip resistance of the

α th slip system according to the saturation-type hardening laws is thus formulated as:

$$\dot{s}^{\alpha} = h_s^{\alpha}\left(1-\frac{s^{\alpha}}{s_s^{\alpha}}\right)\sum_{\alpha=1}^{N_{slip}}\dot{\gamma}^{\alpha} \tag{7}$$

where s_s^{α} and h_s^{α} represent the saturated slip resistance and the hardening rate related to the slip system α, respectively. In addition, in order to capture the complicated interactions of dislocation slip and twinning systems, the hardening equations are given by Salem et al. [26]:

$$h_s^{\alpha} = h_s\left(1+c\left(\sum f^{\beta}\right)^{b}\right) \tag{8}$$

and

$$s_s^{\alpha} = s_{s0} + s_{pr}\left(\sum f^{\beta}\right)^{0.5} \tag{9}$$

where h_s is a material parameter which denotes the initial hardening rate. b and c indicate the hardening index of the twinning system. And s_{s0} represents the saturated value of slip resistance without the influence of all twinning systems, while s_{pr} describes the material parameter to represent the influence of the conventional Hall-Petch effect. Finally, f^{β} illustrates the twin volume fraction of the β th twinning system.

In this research, the rate-dependent approach is adopted in the constitutive model. The shear rate of the α th slip systems could be described by the relationship between shear stress and the slip resistance in the work of Peirce et al. [27]:

$$\dot{\gamma}^{\alpha}=\dot{\gamma}_0\left|\frac{\tau^{\alpha}}{s^{\alpha}}\right|^{1/m}\operatorname{sign}\left(\tau^{\alpha}\right) \tag{10}$$

where s^{α} indicates the slip resistance of the α th slip system. m is a material parameter to represent the strain rate sensitivity. τ^{α} is the RSS on the α th slip system. And $\dot{\gamma}_0$ illustrates a reference slip shear rate, which is assumed to be equal for all the slip systems, as

is adopted in the work of Kalidindi [28]. To describe the twinning shear rate, a similar power law is employed:

$$\dot{\gamma}^{\beta}=\dot{\gamma}_{0}^{\beta}\left(\frac{\tau^{\beta}}{s_{\mathrm{tw}}^{\beta}}\right)^{1/n}, \text{ if } \tau^{\beta}>0; \quad \dot{\gamma}^{\beta}=0, \text{ if } \tau^{\beta}\le 0 \tag{11}$$

where τ^{β} represents the RSS of the β th twinning system and s_{tw}^{β} is the twin resistance in that twinning system. n is the parameter of the strain rate sensitivity in twinning system. And $\dot{\gamma}_{0}^{\beta}$ is a reference to represent the twinning shear rate. Then to conduct the numerical implementation, a detailed Newton-Raphson iteration procedure was discussed in the previous work of Sun et al. [19].

2.2 Incorporation of SE into CP model

The deformation behaviors of materials are closely related to the coupled effects of microstructural transition and macroscopic stress/strain variation. Taking the crystallographic evolution and deformation mechanism into account, the characteristics of mechanical behaviors could be well described and interpreted by using the presented CP model in macro forming process. However, Peng et al. [13] suggested that the behaviors of metallic materials are strongly dependent on the size scale in microforming process, namely SE, which shows a significant difference with the traditional macroforming process. Consequently, the traditional CP model needs to be developed to represent the SE including the grain and geometry SEs.

2.2.1 Surface layer model considering SE

Inhomogeneous deformation characteristics such as stress localization is found to mostly occur in the deformation body with the size scale falling into tens of microns to few hundred microns due to the limited number of grains and geometric dimensions. To address this issue,

extensive theoretical researches including physical models based on continuum mechanics and microscopic constitutive models have been established to accommodate the effect of grain and geometry sizes. The widely used surface layer model assumes that the share of grains in the surface layer becomes greater with the scaling from macro scale to micro one, as shown in Fig. 2 (a). Meanwhile, Peng et al. [13] indicated that the free surface grains are less subjected to the compatibility restriction due to dislocations movement rather than pile-up at grain boundaries, leading to lower resistance and less hardening against the deformation of surface grains. Furthermore, to evaluate the SE at microscale, the ratio of surface grains to inner grains is chosen as a criterion. Consequently, the scale factor λ illustrated by the ratio of surface grains to the total grains in the sample's section is defined as:

$$\lambda = \frac{N_s}{N} \tag{12}$$

where N_s represents the number of surface grains, while N indicates the number of the total grains of the testing sample.

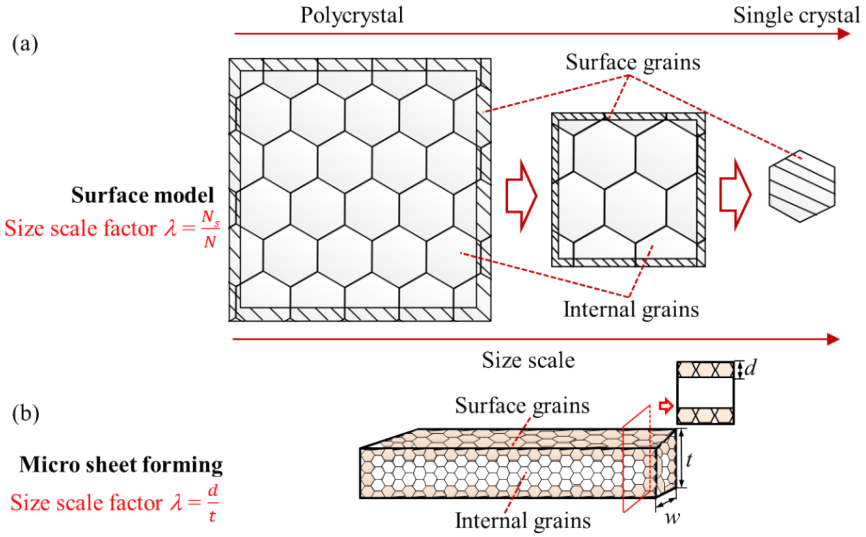

Fig. 2. (a) Grain distribution in a material section with the decreasing size scale; (b) Surface grains and inner grains in the sheet specimen.

2.2.2 Size scaling factor of micro sheet forming

In micro sheet forming process including micro deep drawing, the initial grains distribution is

assumed to be uniform and the grain morphologies are equiaxed, as shown in Fig. 2 (b). In addition, the surface and internal grains are distinguished by color. Fig. 2 (b) assumes that all the diameters of the surface and internal grains in the sheet are *d*. The thickness and width of sheet are represented by *t* and *w*, respectively. Therefore, the quantity of surface grains in the sample section can be calculated approximately:

$$N_s = \frac{wt-(w-2d)(t-2d)}{2d^2} = \frac{w+t}{d} - 2 \tag{13}$$

The quantity of the total grains in a sample section is expressed as:

$$N = \frac{wt}{d^2} \tag{14}$$

Finally, the size scaling factor is obtained as follows [13]:

$$\lambda = \frac{N_s}{N} = \frac{d}{t}\frac{w+t-2d}{w} = \frac{d}{t} \tag{15}$$

2.2.3 SE on slip hardening

With the size scale of materials falling into few hundred microns, Verma and Biswas [21] pointed out that the decreasing grain size leads to the increase of the plastic slip resistance, indicating that grain size plays a significant role in slip hardening. Furthermore, in micro sheet forming process, the geometric SE on strain hardening behaviors should not be neglected. In this research, the size scaling factor considering the influence of grain size and geometry size is thus incorporated into the slip resistance of the slip systems to represent the SE on crystallographic slip.

Based on the framework of the size scale independent conventional CP model mentioned in section 2.1, the saturated slip resistance is suggested to be modified with the proposed size scaling factor, which is motivated by the relation between grain size and dislocation spacing. The relation between the saturated slip resistance s_s and the average dislocation spacing

within an individual crystal is determined as:

$$s_s = \frac{\xi G b_b}{l_f} \tag{16}$$

where ξ represents a material constant, G indicates the shear modulus and b_b means the burger's vector. In addition, l_f is the average spacing between the neighboring forest dislocations. On assuming $K = \xi G b_b$ and differentiating with respect to l_f, the above Eq. (16) is converted to the following:

$$\mathrm{d}s_s = -(\frac{K}{l_f^2})\mathrm{d}l_f \tag{17}$$

The above Eq. (17) represents the relation between the change rate of slip resistance and the average dislocations spacing. A assumption is thus proposed that l_f is proportional to the size scaling factor, namely, $l_f \propto \lambda$, and integrating Eq. (17) from size factor λ_1 to λ_2 as:

$$\int_{s_s^1}^{s_s^2} \mathrm{d}s_s = \int_{\lambda_1}^{\lambda_2} -(\frac{K}{\lambda^2})\mathrm{d}\lambda \tag{18}$$

$$s_s^2 = s_s^1 + K(\frac{1}{\lambda_2} - \frac{1}{\lambda_1}) \tag{19}$$

where s_s^1 indicates the initial slip resistance for the reference size scaling factor λ_1, while s_s^2 represents the slip resistance of λ_2.

Therefore, the relation between the slip resistance and the size scaling factor is given as:

$$s_{size} = K(\frac{1}{\lambda}) \tag{20}$$

where s_{size} describes the size-dependent slip resistance.

Consequently, the saturated value s_s^α associated with the slip system α in Eq. (7) could be modified by incorporating with the size scaling:

$$s_s^\alpha = s_{s0} + s_{size} + s_{pr}\left(\sum f^\beta\right)^{0.5} \tag{21}$$

In this research the SE on twins' nucleation, growth, and further the total hardening has not been taken into account, since twins lamellae struggle to form due to the limitation of sample size at microscopic scale. The twinning resistance s_{tw}^β is assumed to be proportional to slip resistance s^α according to Salem et al [26] in this study. Therefore, the constitutive relations of size dependent CP model of TWIP steel are given in Box 1.

Box 1. Size dependent CP model considering slip and twinning of TWIP steel.

1. Stress - strain relationship

$$\mathbf{T}^e = \mathfrak{R} : \mathbf{E}^e$$

$$\mathbf{E}^e = \frac{1}{2}\left(\mathbf{F}^{e^T} \cdot \mathbf{F}^e - \mathbf{I}\right)$$

$$\mathbf{T}^e = \mathbf{F}^{e^{-1}}\left\{\det\left(\mathbf{F}^e\right)\cdot\boldsymbol{\sigma}\right\}\mathbf{F}^{e^{-\mathrm{T}}}$$

2. Flow rule

$$\text{Slip shear rate}: \dot{\gamma}^\alpha = \dot{\gamma}_0\left|\frac{\tau^\alpha}{s^\alpha}\right|^{1/m}\operatorname{sign}\left(\tau^\alpha\right)$$

$$\text{Twinning shear rate}: \begin{cases} \dot{\gamma}^\beta = \dot{\gamma}_0\left(\dfrac{\tau^\beta}{s_{\mathrm{tw}}^\beta}\right)^{1/m}, \text{ if } \tau^\beta > 0 \\ \dot{\gamma}^\beta = 0, \text{ if } \tau^\beta \le 0 \end{cases}$$

3. Hardening law

$$\dot{s}^\alpha = h_s^\alpha\left(1 - \frac{s^\alpha}{s_s^\alpha}\right)\sum_{\alpha=1}^{N_{slip}}\dot{\gamma}^\alpha$$

$$h_s^\alpha = h_s\left(1 + C\left(\sum f^\beta\right)^b\right)$$

$$s_s^\alpha = s_{s0} + s_{size} + s_{pr}\left(\sum f^\beta\right)^{0.5}$$

$$s_{size} = K\left(\frac{1}{\lambda}\right)$$

$$\text{Size scaling factor } \lambda = \frac{d}{t}$$

A UMAT subroutine was developed based on the modified size dependent crystal plasticity model by using the commercial code of ABAQUS. The detailed numerical implementation process was presented as the flow chart in Fig. 3.

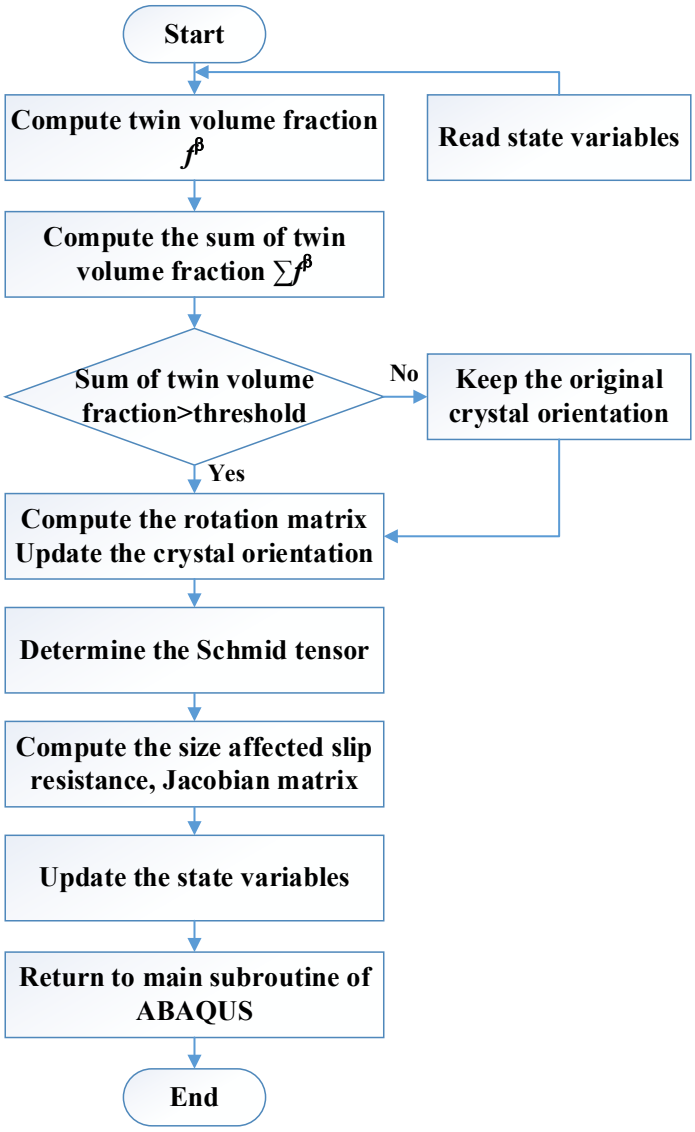

Fig. 3. The flow chart of numerical algorithm into implicit FEM.

2.3 Evaluation of the size dependent CP model

To evaluated the reliability of the proposed size dependent crystal plasticity model applied in the micro deep drawing process, the comparison of the mechanical properties measured in the micro tensile test and calculated by CPFEM was conducted.

In-situ tension tests were carried out on a stretching device loading on FEI Quanta 250 SEM

at room temperature shown in Fig. 4. The converted strain rate obtained from the displacement mode is approximately 7.5×10^{-5} s^{-1}. Then, FE simulations of the micro tensile test were conducted based on a virtual polycrystalline microstructure using the proposed CP model. The final values adopted for a series of material parameters for TWIP steel together with elastic tensors are determined and illustrated in Table 1. The methods for determining the material parameters refer to the study of Guo et al. [29]. The detailed analysis of the plastic parameters sensibility has been given in the previous work by Sun et al. [30]. Consequently, the comparison of the true stress-strain curves determined by experiment and simulation with the thickness of 100 μm and average grain size of 30 μm is shown in Fig. 5. It could be noted that there is a good fitting to the experimental results in terms of the true stress-strain curve. However, it is observed that a deviation occurs before the strain of 0.2, which could be illustrated that a large amount of deformation twinning occurred within the grains in the in-situ micro tensile test whereas the effect of deformation twinning had not been incorporated until the saturated value of twin volume fraction reaching the threshold in the CPFEM simulation.

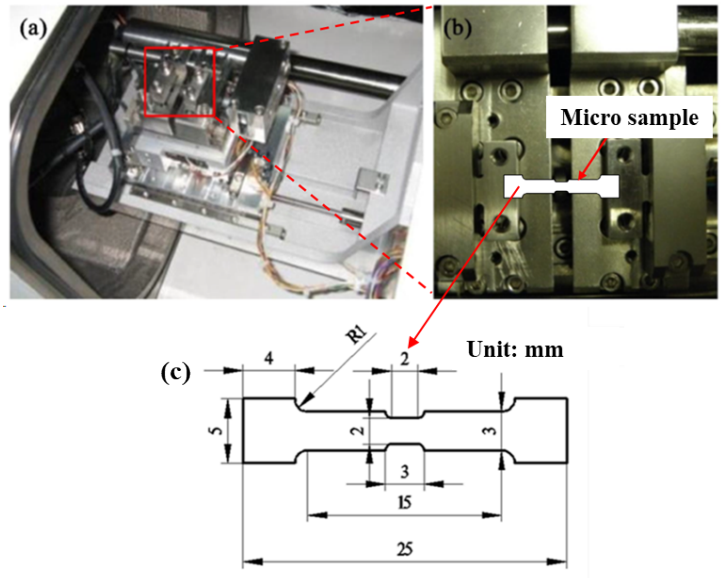

Fig. 4. In-situ tensile apparatus (a) with its enlarged part (b) and the dimension diagram of

micro sample (c).

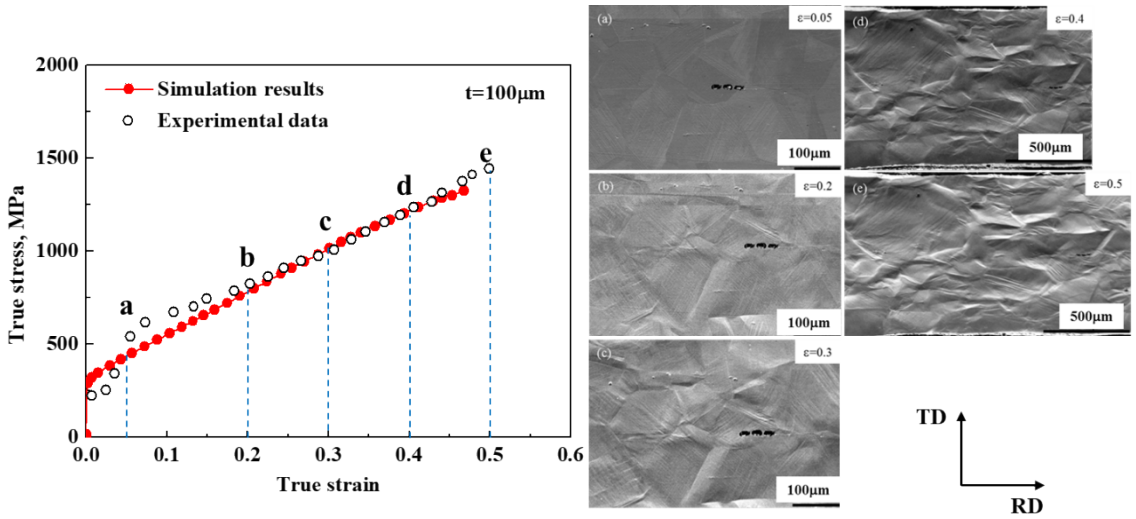

Fig. 5. Comparison of the true stress-strain curves determined by experiment and simulation with the thickness of 100 μm and average grain size of 30 μm. The SEM micrographs of the in-situ tensile for specimens strained from 0.05 to 0.5 is given in (a)-(e) respectively.

Table 1. Material parameters in the constitutive relations calibrated for TWIP steel.

Initial hardening rate of slip system h_s (MPa)	400
Material constant K	300
Hardening index of twinning b	2
Hardening coefficient of twinning c	10
Effect of Hall-Petch mechanism s_{pr} (MPa)	400
Initial slip resistance s_0^{α} (MPa)	120
Initial twinning resistance s_0^{β} (MPa)	139.2
Elastic constant C_{11} (GPa)	198
Elastic constant C_{12} (GPa)	125
Elastic constant C_{44} (GPa)	122
Rate sensitivity coefficient m	0.02
Reference shear rate $\dot{\gamma}_0$ (s^{-1})	0.001

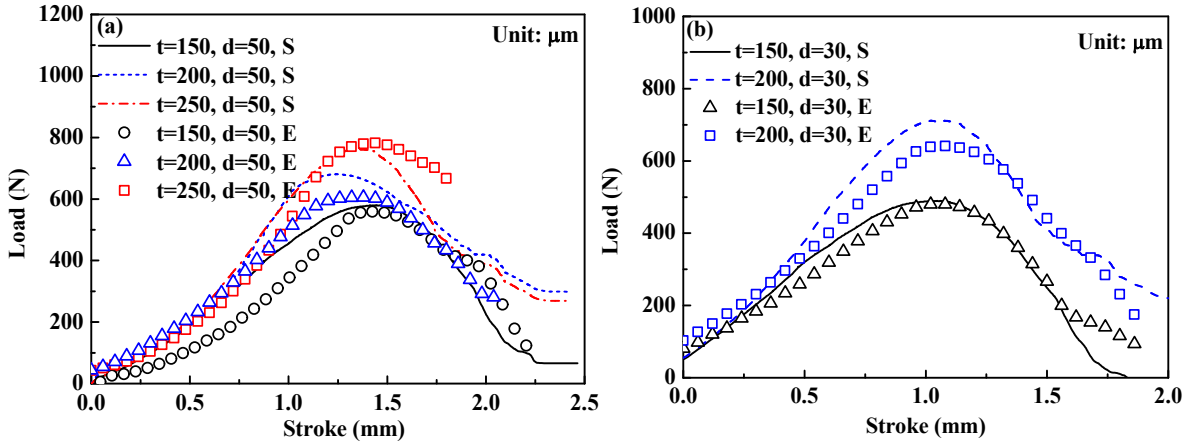

Fig. 6. Comparison of the load-stroke curves determined by experiment (E) and simulation (S) with different grain sizes (*d*) and thicknesses (*t*).

The SE in micro deep drawing process can be calibrated via comparison of the loads measured in experiments and calculated by CPFEM. From Fig. 6 (a) and (b), it is found that there exist deviations between the load-stroke curves determined by simulation and experiment, since the measured data strongly depends on the great variation in crystallographic orientation and the transient non-uniform stress/strain state during micro deep drawing processing. However, the obvious SE indicated by the increase of forming force with the decreasing of size scaling factor for the grain size of 50 and 30 μm can still be observed in Fig. 6 (a) and (b), respectively. In addition, the simulated and measured curves and the occurrence of the second load peaks exist at the stage with the stroke between 1.5 and 2 mm, which is believed to be caused by the ironing effect at the later stage of the drawing process [31, 32].

3. Experimental procedure

3.1 Material preparation and characterization

In this research, the case study material, Fe-Mn-Si-Al TWIP steel with the chemical composition listed in Table 2, was manufactured by a vacuum induction furnace. The testing

micro blanks with the given radius and different thickness shown in Fig. 7 (a) were cut from the TWIP steel sheet. These micro workpieces were annealed at 600, 700 and 900 °C, respectively, with a fixed holding time of 1 hour in a protective argon condition to avoid oxidation and then followed by air cooling.

Table 2. Chemical composition (in weight percent) of Fe-30Mn-3Si-2Al TWIP steel.

C	Mn	Si	Al	S	P	Ti	Fe
0.11	30.5	2.88	2.34	0.013	0.007	≤0.01	Bal.

Grain morphologies of the testing samples were characterized by EBSD technique after annealing with different temperatures. The analysis of grain morphology demonstrated the equiaxed grains with the average grain sizes of 25, 30 and 50 μm (excluding twins) for the homogenized samples annealed at 600, 700 and 900 °C, respectively, as shown in Fig. 7 (b).

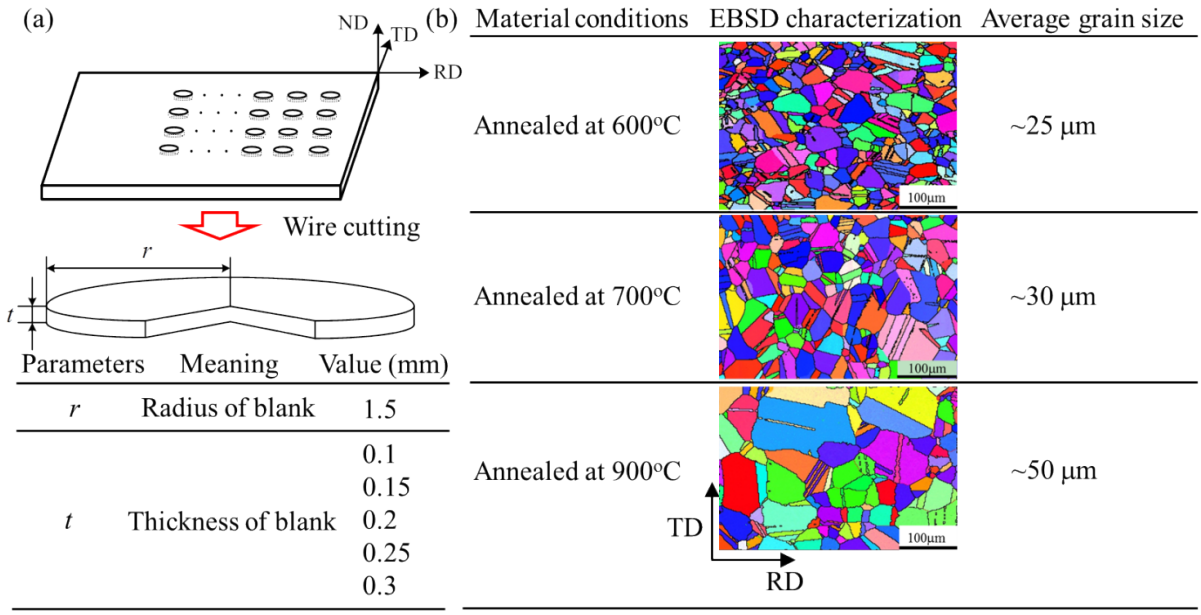

Fig. 7. (a) Preparation process and parameters of test piece; (b) Average grain sizes of samples annealed at different temperatures and characterized by EBSD.

3.2 Set-up of micro deep drawing process

The schematic of micro drawing process is illustrated in Fig. 8 (a), and the detailed parameters and dimensions of tooling sets is given in Table 3. Particularly, the diameters of drawing punch with domed bottom and drawing die are 1.3 mm and 1.7 mm respectively. In addition, the unilateral drawing clearance between punch and die is 0.2 mm, the same as the sheet thickness. The actual detailed schematic of testing platform, tooling sets of micro deep drawing for these micro blanks are designed and given in Fig. 8 (b). Subsequently, the micro deep drawing tests were conducted in an MTS testing machine with a load cell of 30 KN for measuring the punch stroke and deformation load. The interface between tooling sets and workpiece was lubricated with machine oil. To ensure the good formability of defect-free micro cups, a low velocity of punch displacement is approximately 0.02 mm/s [33].

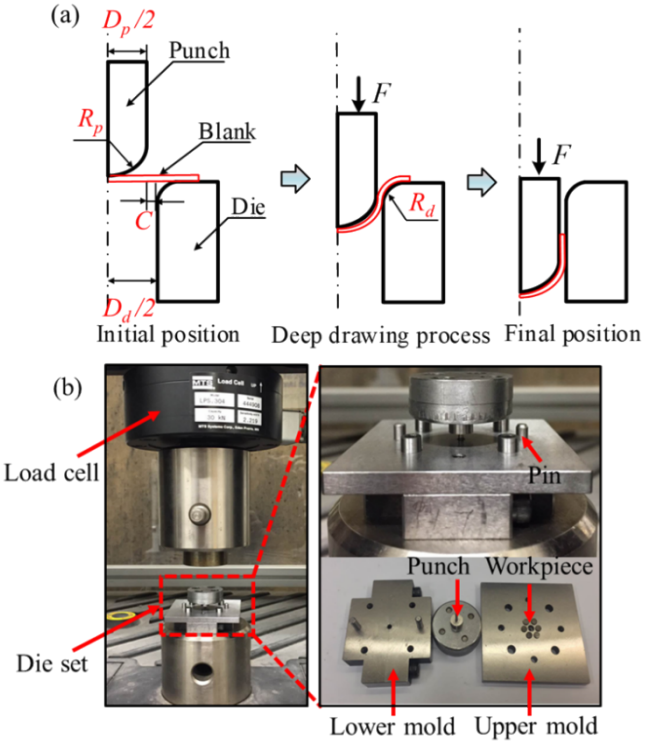

Fig. 8. (a) Schematic of micro deep drawing process; (b) Testing platform and tooling set in micro deep drawing process.

Table 3. Dimensions and parameters of tooling sets.

Parameters	Meaning	Value (mm)
D_p	Diameter of drawing punch	1.3
D_d	Diameter of drawing die	1.7
R_p	Radius of drawing punch	0.65
R_d	Radius of drawing die	0.5
C	Unilateral drawing clearance	0.2

4 Size and grain orientation affected earing evolution

4.1 Development of FE model for micro deep drawing

In order to investigate the unique features of the earing of TWIP steel at micro scale, the conventional FE model of macroscopic deep drawing process was established to be provided as a comparison although the evolution of earing characteristics of TWIP steel were simulated extensively at macro scale [34]. A brief description of the FE model for deep drawing process was introduced as follows. Due to the sufficiently high symmetry, only a quarter of the blank meshed with C3D8 type was considered for deep drawing analysis. The tooling components including punch and die were modelled as analytical rigid bodies. The contact condition between the workpiece and die, as well as that between the workpiece and the binder plate in tangential direction are assumed to be govern by the Coulomb friction model with a friction coefficient of 0.1, while the friction coefficient between the punch and the specimen is defined as 0. The upper surface of the punch was subjected to the drawing force and the punch only moved along the y axis. The aim of the abovementioned FE model is to study the earing characteristics at macro scale.

At micro scale, due to the orthotropic symmetry of samples, simulations of micro deep drawing were conducted using the model with a quarter of the blank and tool set. The FE

model with mesh configuration of the specimen prior to loading is given in Fig. 9. Particularly, the virtual polycrystalline microstructure including grain morphology and grain orientations is generated using an open-source software package named Neper construct as the Voronoi tessellation model [35]. This representative volume element model containing deformation twinning within matrix considering the crystallographic orientation and morphological feature was employed to reconstruct the polycrystalline microstructure, as shown in Fig. 9. The element density is increased along the blank to its center to acquire a favorable accuracy of the cup edge. In the one-quarter model, the blank was meshed with 9215 C3D4 elements, and the punch as well as the die were regards as rigid bodies, which were modeled using 265 and 627 R3D4 elements respectively. In micro deep drawing process, the occurrence probability of wrinkling is relatively low due to the small specimen size. In addition, since the blank holder might raise concerns that the calculated earing profiles are caused by buckling rather than by the anisotropy of the material, the blank holder was not used in the tooling set. The polycrystalline orientations of the blank were assigned randomly based on the experimental data.

In micro deep drawing model, the friction coefficient between blank and tooling set is one of the most crucial parameters, which has a more significant influence on the cup formability and production quality compared with the conventional scale. In this developed FE model, the Coulomb friction coefficient μ was assumed to be 0.1 to describe the friction interaction between the blank and the punch. Rabbe et al. [36] demonstrated that the conventional J_2-based continuum plasticity simulation of earing shape in deep drawing process represents a strong dependence on friction coefficient, which is generally stronger than CP model. In these simulations, however, the primary research was to investigate the SE on the earing characteristics including relative ear height and shape by using the size-dependent CP model from the view point of crystallographic evolution rather than process parameters. Therefore,

only a fixed friction coefficient, namely μ=0.1 between the blank and the punch was adopted in the simulation.

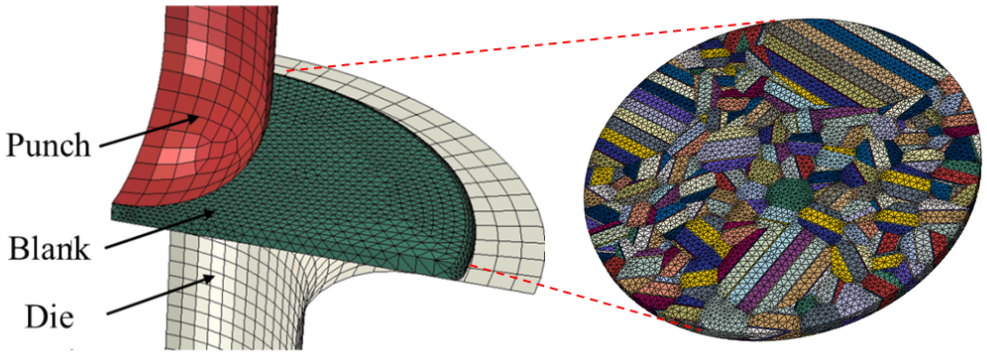

Fig. 9. FE modelling of micro deep drawing process.

4.2 Experiment of size effect on earing at micro scale

Fig. 10 (a) shows the geometric characteristics of the formed cups made from the materials with different thicknesses and annealed at the temperature of 700 and 900 °C. A magnified and detailed feature of the cup formability including earing profile and fracture was characterized by SEM scanning, as shown in Fig. 10 (b). With the decrease of thickness, the earing is more significant. The distribution of grains in the sheet with the thickness of 0.2 mm is presented, which is more uniform than that of the materials with the thickness of 0.1 and 0.15 mm. Therefore, the earing mainly caused by uneven grains distributions and their orientations is more likely to occur in the cases with thinner thickness. In addition, for the TWIP sheet annealed at 900 °C, the larger grains size leads to the inhomogeneous deformation more easily in the case of the same sample size, which causes the irregular geometry of the drawn cups [37]. Consequently, the obvious earing profile appeared in the case with the larger size scaling factor shown in Fig. 10 (b).

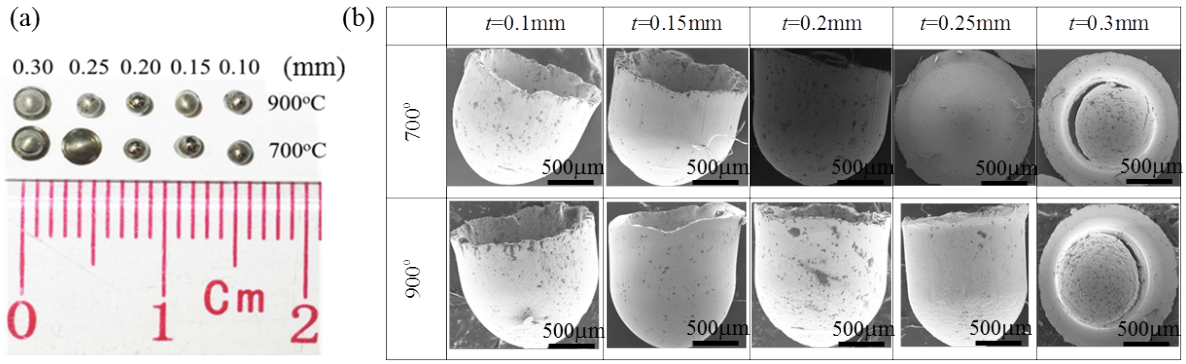

Fig. 10. (a) Comparison of the different thickness size-scaled cups made from the materials with different annealed temperatures, (b) SEM images of the different scaled micro parts.

To articulate the SE on earing profile, different values of λ were employed into the size-dependent CP simulation. The comparison of the simulated and experimental earing characteristics was provided with the size scaling factors of 1/2 and 1/4 and the annealed temperature of 900 °C, as shown in Fig. 11. The distinct earing types and amounts including two 0°/180° and four 0°/90° appeared with the λ=1/2 and λ=1/4, respectively. For the randomly distributed crystal orientations, the varying earing characteristics under the different size scaling factors are attributed to grain and geometry sizes. With the increasing tendency of λ, viz., the increasing grain size and decreasing geometry size, the microstructure of the sample is equivalent to single crystal case in the extreme scenario. The pronounced planar anisotropy would take place, which could generate the obvious earing profiles.

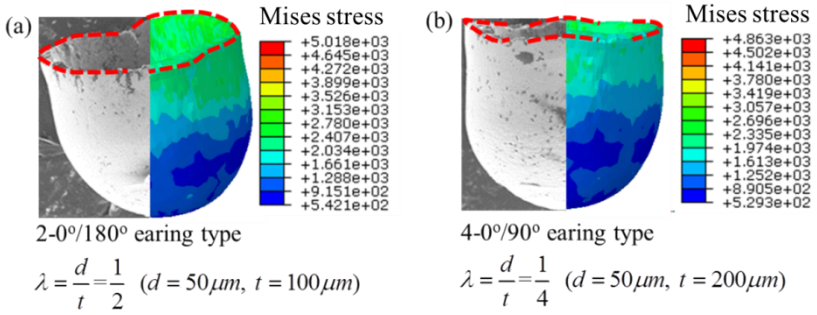

Fig. 11. Comparisons of the experimental and simulated earing profiles with the size scaling factor 1/2 (a) and 1/4 (b).

4.3 Effect of initial grain orientation on earing evolution

4.3.1 Earing characteristics at macro scale

Since the deformation texture leading to anisotropy plays an important role in the earing formation, the effect of the starting grain orientations on earing was investigated at macro scale for prediction of earing profiles subsequently. The initial three types of grain orientations including Goss {011}<100>, Cube {001}<100> and Brass types {011}<211>, which belong to the common grain orientations in FCC metallic materials, were employed in CP simulations to represent the relative earing heights in the cup-drawn TWIP steel samples.

The relative earing height and earing types caused by the abovementioned three initial grain orientations were simulated and given in Fig. 12 (a). It is noted that there were 6-0^o/60^o-earing-type and 4-0^o/90^o-earing-type being produced influenced by the Brass type and Cubic type of initial orientations, respectively. Meanwhile, the earing type under the effect of the Goss was presented a quasi-4-0^o/90^o-type. In addition, it is observed that the earing profile generated by the Cubic type orientation exhibits a symmetrical distribution, in contrast with that calculated by the Goss and Brass types.

The Lankford value (r value) which is defined as the ratio of the true width strain to true thickness strain was measured as a significant parameter to represent the material anisotropy at macro scale. As is shown in Fig. 12 (b), the r value of the Cube and Goss types present trends relatively less than that of the Brass type which indicates that the thickness strain gains importance at the expense of the width strain under the Brass type.

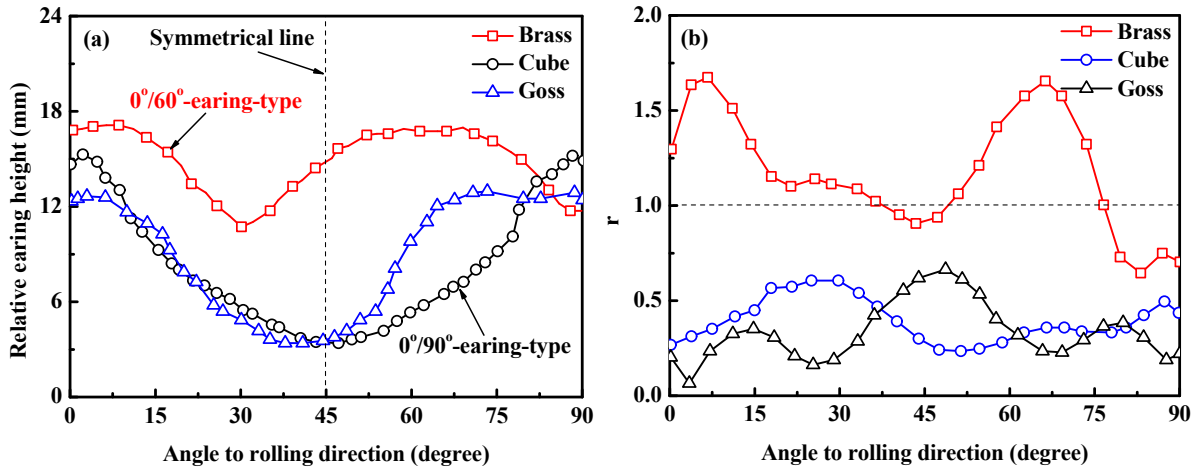

Fig.12. Earing characteristics for different initial textures: (a) cup height, (b) *r* value.

4.3.2 Prediction of earing at micro scale

Compared with the earing characteristics at macro scale, the evolution of earing at micro scale caused by the abovementioned initial grain orientations are analyzed according to the slip and twinning mechanisms. Therefore, the interactive influence of the size effect and crystal texture is considered to explore the orientation-dependent anisotropy.

As shown in Fig. 13 (a), it is observed that the earing profile generated by the Cubic type orientation exhibits a symmetrical distribution which is similar to that calculated at macro scale. To articulate the influence of varying grain orientations on earing profiles quantitatively, the earing rate calculated by CP simulations with Brass, Cube and Goss orientations are shown in Fig. 13 (b). At micro- and macro scale, the Goss orientation has a more significant influence on earing height than that of the Brass and Cubic types. Particularly, it is noted that the earing rate at micro scale is obviously higher than that calculated at macro scale. The earing behavior can thus be reduced by weakening or avoiding the strong Goss-type orientations of the TWIP steel sheets. To address this issue, the evolutions of deformation mechanisms including slip and twin activities were investigated in

the following sections.

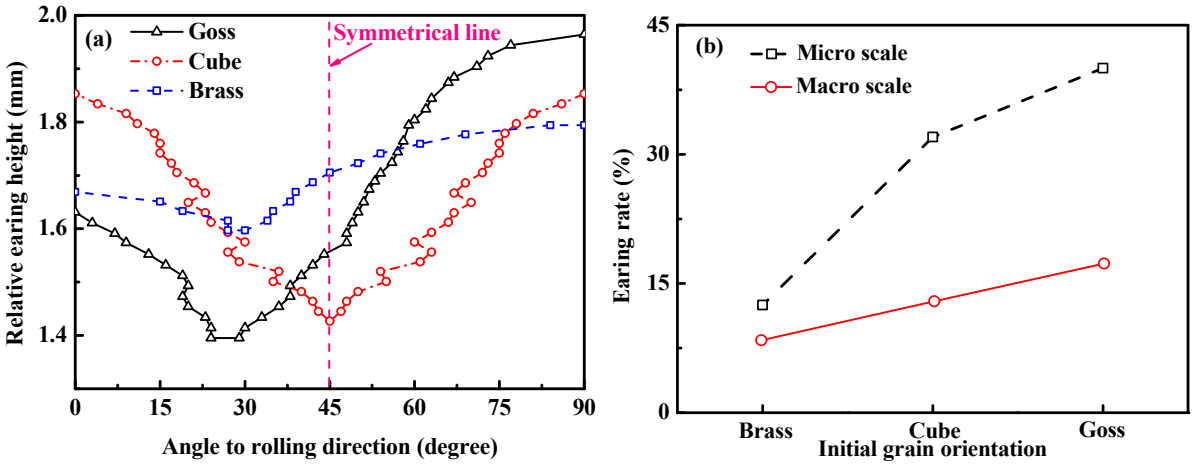

Fig. 13. Earing characteristics of samples with different initial grain orientations: (a) cup height and (b) earing rate.

Fig. 14 shows the evolution of the relative activities of various slip, and twinning mechanisms with different true strains for each orientation. For the Goss orientation, the asymmetric activated slip system a_2 exhibited a larger and sustained increasing tendency of the slip increment than that of the other slip systems, which indicates a_2 is a dominant slip system in cup drawing process, as shown in Fig. 14 (a). However, in Fig. 14 (d), only twinning system u_1 shows an obvious increasing trend. The twinning increment gradually reaches the saturated value of 0.025. This illustrates the well-formed cups with good ductility may be caused by the activation of the slip mode, which provides stable plastic deformation. Therefore, from the view point of deformation mechanism, the influence of Goss orientation on the earing shape could be explicated and attributed to the asymmetric activated slip mechanism rather than twinning due to the amount of slip and twinning activation in the micro cup drawing process.

Table 4. Twelve slip systems and twelve twinning systems of TWIP steel.

Deformation	Symbols	Plane	Direction	Symbols	Plane	Direction
Slip systems	a_1	(111)	$[01\bar{1}]$	b_1	$(\bar{1}\bar{1}1)$	$[0\bar{1}\bar{1}]$
	a_2	(111)	$[\bar{1}01]$	b_2	$(\bar{1}\bar{1}1)$	$[101]$
	a_3	(111)	$[1\bar{1}0]$	b_3	$(\bar{1}\bar{1}1)$	$[\bar{1}10]$
	c_1	$(\bar{1}11)$	$[01\bar{1}]$	d_1	$(1\bar{1}1)$	$[0\bar{1}\bar{1}]$
	c_2	$(\bar{1}11)$	$[101]$	d_2	$(1\bar{1}1)$	$[\bar{1}01]$
	c_3	$(\bar{1}11)$	$[\bar{1}\bar{1}0]$	d_3	$(1\bar{1}1)$	$[110]$
Twinning systems	t_1	(111)	$[11\bar{2}]$	u_1	$(\bar{1}\bar{1}1)$	$[112]$
	t_2	(111)	$[\bar{2}11]$	u_2	$(\bar{1}\bar{1}1)$	$[2\bar{1}1]$
	t_3	(111)	$[1\bar{2}1]$	u_3	$(\bar{1}\bar{1}1)$	$[\bar{1}21]$
	v_1	$(\bar{1}11)$	$[211]$	w_1	$(1\bar{1}1)$	$[121]$
	v_2	$(\bar{1}11)$	$[12\bar{1}]$	w_2	$(1\bar{1}1)$	$[21\bar{1}]$
	v_3	$(\bar{1}11)$	$[1\bar{1}2]$	w_3	$(1\bar{1}1)$	$[\bar{1}12]$

As shown in Fig. 14 (b), the slip activity for Cubic orientation during the drawing process is symmetrically distributed. All the twinning systems are actually active albeit different twinning increments for each twinning system. Similarly, the twinning activities manifested less dominant compared to the slip activities in terms of the amount of activation. Therefore, the symmetric distributed slip activities lead to the earing symmetrically. For the case of Brass type, the activation and evolution of slip and twinning are similar to that of Goss type. However, the amount of slip and the twinning increment of Goss orientation are larger than that of Brass orientation. The earing rate influenced by the Goss orientation is thus higher than that of Brass, despite the analogous earing positions of Goss and Brass orientations.

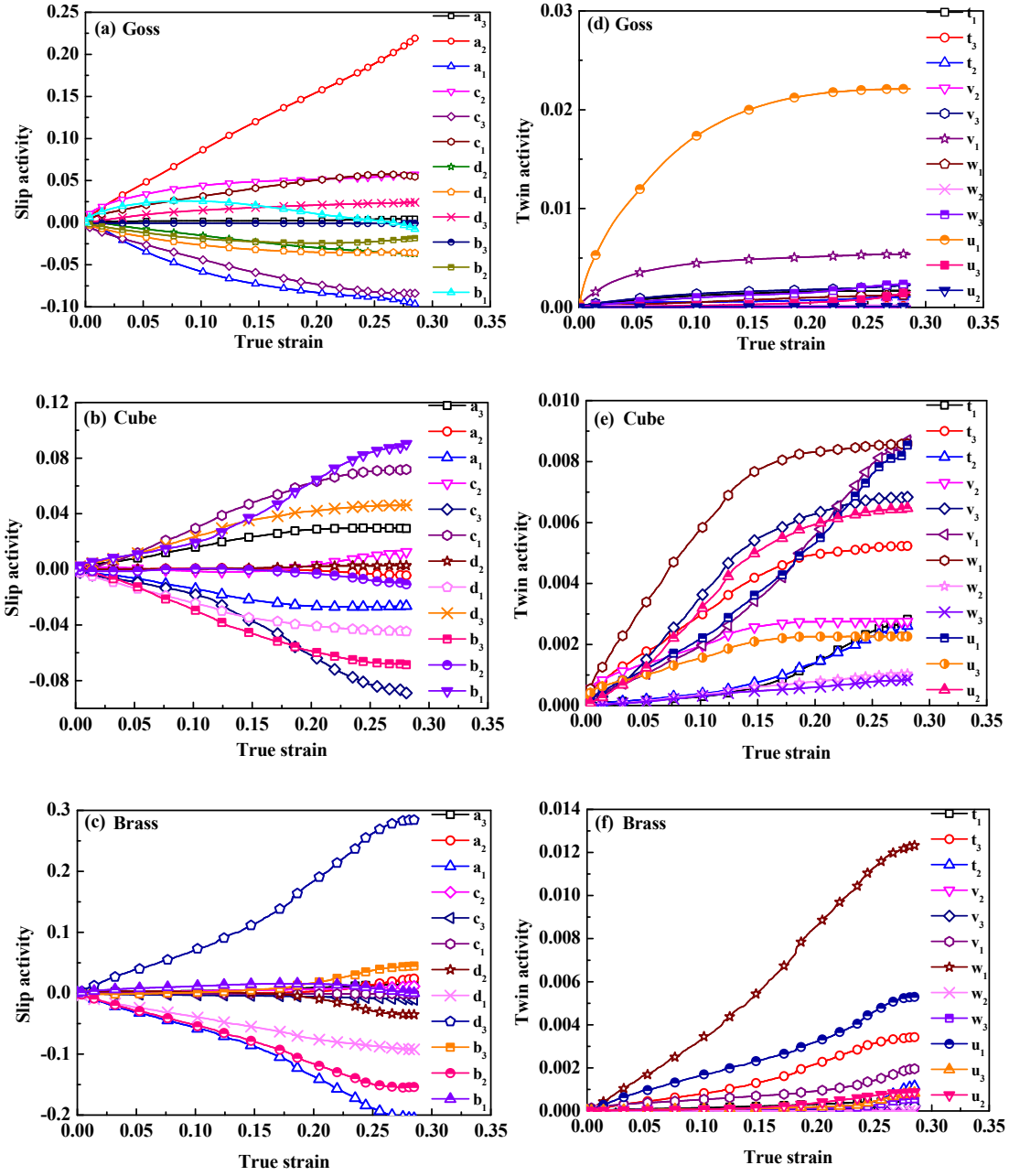

Fig. 14. (a-f) Activated slip and twinning systems of the samples with Goss- Cube- and Brass-type grain distributions during micro deep drawing process.

To illustrate the evolution of twinning hardening under the initial Goss, Cube and Brass orientations during the earing process, the twin volume fractions were predicted as a function of the applied strain and shown in Fig. 15. In addition, the evolution of twin volume fraction with the orientations of Goss and Brass shows the similar trends to reach the saturated value,

except the order of magnitude, in contrast to the increasing tendency of the twin volume fraction with the orientation of Cubic type. It was informative to note that the Cubic orientation plays a key role in producing much twinning compared to the scenario of the Goss and Brass orientations.

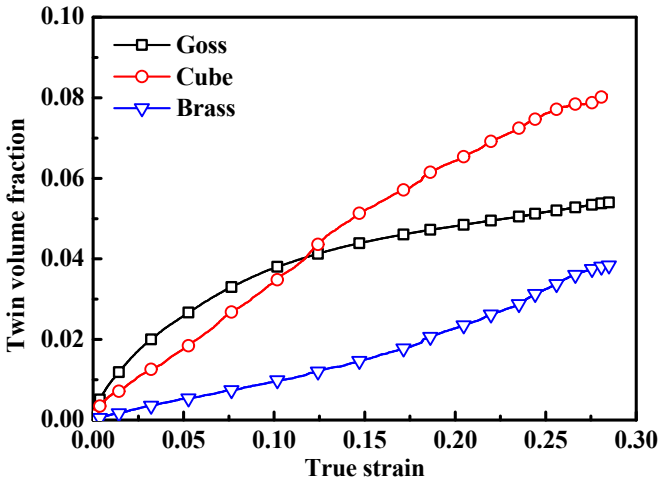

Fig. 15. Evolution of the twin volume fraction with different initial grain orientations.

5. Conclusions

By using an annealed high strength TWIP sheet as a case study material for micro-deep drawing, the contributions of grain orientation and size effect to the evolution of earing and micro deep drawing behavior of the steel and the underlying slip and twinning activities in the process are quantitatively investigated based on the experiment and numerical simulation. The influence of the initial grain orientation, grain and geometry sizes on earing characteristics at micro scale is presented. The main concluding remarks are summarized in the following:

(1) A physically motivated size-dependent CP model incorporating the ratio of grain size to geometry size based on surface layer model is proposed to investigate the evolution of earing considering the size effect in micro deep drawing process and to predict the influence of the geometrical size and grain orientation on the earing profiles of polycrystalline TWIP steel.

(2) By using the elaborately designed micro deep drawing of TWIP micro sheets, the influence of size scaling factor, which is considered as an approach to representing the SE, on earing SE is articulated. It is found that the obvious earing profile occurs in the case with the larger size scaling factor. In addition, the earing shape is strongly affected by the size scaling factor.

(3) The influence of initial grain orientation including Goss, Cube and Brass on earing profile is explained that the earing height caused by the Goss type is larger than that of the Cube and Brass ones. Moreover, the asymmetric distribution of earing profile is induced by the Goss and Brass orientations, while the Cubic type leads to the symmetric distribution of earing. This is mainly attributed to the symmetric evolution of slip activities than that of twinning activities, since the activated quantity of twinning volume fraction is much smaller.

(4) Crystal plasticity modelling is efficient in analysis of micro deep drawing of TWIP steel and provides an in-depth understanding and insight into the deep drawing process when it is used together with physical experiment.

Acknowledgements

The authors would like to thank the supports to this research from the National Natural Science Foundation of China (Nos. 51575039 and 51575465), NSAF (No. U1730121), and the project of B-Q55M (152792/16E) from the RGC of Hong Kong Government.

References

[1] Vollertsen F, Hu Z, Schulze NH, Theiler C. State of the art in micro forming and investigations into micro deep drawing. J. Mater. Process. Technol. 2004; 151: 70-79.

[2] Krishnan N, Cao J, Dohda K. Study of the size effects on friction conditions in microextrusion—part i: microextrusion experiments and analysis. J. Manuf. Sci. Eng. 2007; 129: 669-676.

[3] Parasiz SA, Kinsey B, Krishnan N, Cao J, Li M. Investigation of deformation size effects during microextrusion. J. Manuf. Sci. Eng. 2016;129, 690-697.

[4] Fu MW, Chan WL. A review of the state-of-the-art microforming technologies, Int. J. Adv. Manuf. Tech. 2013; 67: 2411-2437.

[5] Fu MW, Yang B, Chan WL. Experimental and simulation studies of micro blanking and deep drawing compound process using copper sheet. J. Mater. Process. Technol. 2013; 213: 101-110.

[6] Fu MW, Wang JL, Korsunsky AM. A review of geometrical and microstructural size effects in micro-scale deformation processing of metallic alloy components, Int. J. Mach. Tools Manuf. 2016; 109: 94-125.

[7] Cheng C, Wan M, Meng B, Fu MW. Characterization of the microscale forming limit for metal foils considering free surface roughening and failure mechanism transformation, J. Mater. Process. Technol. 2019; 272: 111-124

[8] Tang WQ, Huang SY, Li DY, Peng YH. Mechanical anisotropy and deep drawing behaviors of AZ31 magnesium alloy sheets produced by unidirectional and cross rolling. J. Mater. Process. Technol. 2015; 215: 320-326.

[9] Saotome Y, Yasuda K, Kaga H. Microdeep drawability of very thin sheet steels. J. Mater. Process. Technol. 2001; 113: 641-647.

[10] Chan WL, Fu MW. Experimental studies and numerical modeling of the specimen and grain size effects on the flow stress of sheet metal in microforming. Mater. Sci. Eng. A 2011; 528: 7674-7683.

[11] Xu ZT, Peng LF, Yi PY, Lai XM. An investigation on the formability of sheet metals in the micro/meso scale hydroforming process. Int. J. Mech. Sci. 2019; 150 265-276.

[12] Molotnikov A, Lapovok R, Davies CHJ, Cao W, Estrin Y. Size effect on the tensile strength of fine-grained copper. Scr. Mater. 2008; 59:1182-1185.

[13] Peng LF, Lai XM, Lee HJ, Song JH, Ni J. Analysis of micro/mesoscale sheet forming process with uniform size dependent material constitutive model. Mater. Sci. Eng. A 2009; 526: 93-99.

[14] Geißdörfer S, Engel U, Geiger M. FE-simulation of microforming processes applying a mesoscopic model. Int J. Mach. Tools Manuf. 2006; 46: 1222-1226.

[15] Tôth LS, Lapovok R, Molotnikov A, Gu C, Fundenberger JJ, Davies CHJ. Texture evolution during micro-drawing of ultrafine grained copper. Mater. Sci. Eng. A 2010; 527: 4633-4640.

[16] Tjahjanto DD, Eisenlohr P, Roters F. Multiscale deep drawing analysis of dual-phase steels using grain cluster-based RGC scheme. Modelling Simul. Mater. Sci. Eng. 2015; 23: 045005.

[17] Walde T, Riedel H. Simulation of earing during deep drawing of magnesium alloy AZ31. Acta Mater. 2007; 55: 867-874.

[18] Tikhovskiy I, Raabe D, Roters F. Simulation of earing during deep drawing of an Al-3% Mg alloy (AA 5754) using a texture component crystal plasticity FEM. J. Mater. Process. Technol. 2007; 183: 169-175.

[19] Sun CY, Guo N, Fu MW, Wang SW. Modeling of slip, twinning and transformation induced plastic deformation for TWIP steel based on crystal plasticity, Int. J. Plast. 2016; 76: 186-212.

[20] Kocks UF, Mecking H. Physics and phenomenology of strain hardening: the FCC case. Prog. Mater.Sci. 2003; 48: 171-273.

[21] Verma RK, Biswas P. Crystal plasticity-based modelling of grain size effects in dual phase steel, Mater. Sci. Techno. 2016; 32: 1553-1558.

[22] Acharya A, Beaudoin AJ. Grain-size effect in viscoplastic polycrystals at moderate strains, J. Mech. Phys. Solids 2000; 48: 2213-2230.

[23] Zhang HM, Dong XH. Physically based crystal plasticity FEM including geometrically necessary dislocations: Numerical implementation and applications in micro-forming. Comp. Mater. Sci. 2015; 110: 308-320.

[24] Cheong KS, Busso EP, Arsenlis A. A study of microstructural length scale effects on the behaviour of FCC polycrystals using strain gradient concepts, Int. J. Plast. 2005; 21: 1797-1814.

[25] Kalidindi SR, Bronkhorst CA, Anand L. Crystallographic texture evolution in bulk deformation processing of FCC metals, J. Mech. Phys. Solids 1992; 40: 537-569.

[26] Salem A, Kalidindi SR, Semiatin S. Strain hardening due to deformation twinning in α-titanium: Constitutive relations and crystal-plasticity modeling, Acta Mater. 2005; 53: 3495-3502.

[27] Peirce D, Asaro R, Needleman A. An analysis of nonuniform and localized deformation in ductile single crystals, Acta metal. 1982; 30:1087-1119.

[28] Kalidindi SR. Modeling anisotropic strain hardening and deformation textures in low stacking fault energy FCC metals, Int. J. Plast. 2001; 17: 837-860.

[29] Guo N, Sun CY, Fu MW, Han MC. Misorientation-dependent twinning induced hardening and texture evolution of TWIP steel sheet in plastic deformation process. Metals 2017; 7: 348.

[30] Sun CY, Huang J, Guo N, Yang J, Wang B. Sensitivity analysis of hardening parameters in the crystal plasticity model exhibiting deformation twinning. Chin. J. Eng. 2015; 37: 1076-1083.

[31] Neto DM, Oliveira MC, Alves JL, Menezes LF. Influence of the plastic anisotropy modelling in the reverse deep drawing process simulation. Mater. Des. 2014; 60: 368-379.

[32] Sherbiny M E, Zein H, Abd-Rabou M, Shazly ME. Thinning and residual stresses of

sheet metal in the deep drawing process. Mater. Des. 2014; 55: 869-879.

[33] Guo N, Sun CY, Fu M W. Size effect affected deformation characteristics in micro deep drawing of TWIP domed-bottom cups. Procedia Eng. 2017; 207:2072-2077.

[34] Sun CY, Wang B, Politis DJ, Wang LL, Cai Y, Guo XR, Guo N. Prediction of earing in TWIP steel sheets based on coupled twinning crystal plasticity model. Int. J. Adv. Manuf. Tech. 2017; 89: 3037-3047.

[35] Quey R, Dawson PR, Barbe F. Large-scale 3D random polycrystals for the finite element method: Generation, meshing and remeshing. Comput. Methods Appl. Eng. 2011; 200: 1729-1745.

[36] Raabe D, Wang Y, Roters F. Crystal plasticity simulation study on the influence of texture on earing in steel. Comp. Mater. Sci. 2005; 34: 221-234.

[37] Wang JL, Fu MW, Shi SQ. Influences of size effect and stress condition on ductile fracture behavior in micro-scaled plastic deformation. Mater. Des. 2017; 131: 69-80.